Quantum Efficiency Enhancement versus Reduced Power Conversion Efficiency in Graphene/MoS_2/n-Si Cells

Omar S. Omar[†]

Department of Physics, College of Science, University of Duhok, Duhok,
Kurdistan Region - F.R. Iraq

***Abstract*—In this study, we examined the performance of a vertically stacked solar cell made of graphene, monolayer MoS_2, and n-type silicon, which combines the exceptional transparency and high carrier mobility of graphene with the light absorption capabilities of MoS_2 and the proven photovoltaic response of silicon. The solar cell recorded the maximum external quantum efficiency (EQE) of 60% at ~660 nm, significantly higher than the previously recorded 44% EQE for the Mo_2/n-Si junction alone. Despite this improvement in the EQE, the power conversion efficiency fell from 2.46% to 1.6% after graphene integration, owing to higher interfacial recombination and series resistance. These results clarify the potential and inherent trade-offs of implementing 2D/2D/3D hybrid structures for efficient sunlight harvesting, paving the way for interface design solutions to fully exploit their capabilities.**

***Index Terms*—2D materials, Graphene, Heterostructure solar cell, Monolayer MoS_2, N-type silicon.**

I. Introduction

After the discovery of graphene, significant attention has been paid to integrating it with other two-dimensional materials into optoelectronic devices; such attention has risen due to the exceptional structural, electrical, and optical characteristics of these materials. Graphene and molybdenum disulphide monolayers (MoS_2) emerged as promising candidates for next-generation photovoltaic and energy conversion applications. Their flexibility, high carrier mobility, and ability to form van der Waals heterostructures make them ideal components for Schottky solar cells. In such a device, interfacial engineering has the crucial role in enhancing carrier separation and transport, directly affecting overall device performance (Ferrari, et al., 2015).

MoS_2 has a layer-dependent band gap, transitioning from an indirect (~1.3 eV) in bulk material to a direct band gap (~1.8 eV) in a monolayer (Mak, et al., 2010). With the direct band gap in the visible range, MoS_2 exhibits enhanced photon absorption and efficient exciton generation (Splendiani, et al., 2010), in addition to its charge separation efficiency with a high conduction band offset relative to silicon, allowing electron injection and minimizing recombination losses (Tsai, et al., 2014), along with its stability under ambient conditions, all of which contribute to its suitability for solar cell applications (Amani, et al., 2015).

Graphene, a monolayer of carbon atoms, has gained interest due to its outstanding optoelectronic properties, with carrier mobility reaching up to ($>10^5$ $cm^2/V{\cdot}s$) and near-perfect transparency (~97% transmittance), making it a suitable electrode for optoelectronic devices (Du, et al., 2008; Novoselov, et al., 2012; Tao, et al., 2020). Despite these advantages, graphene is a semimetal with zero band gap, which influences charge transport dynamics at heterojunction interfaces by introducing charge screening effects and recombination losses. Careful engineering of the graphene/MoS_2 interface is required to maximize the benefits while mitigating undesirable transport limitations (Rao, et al., 2019).

In 2D/3D hybrid structures, when combining graphene, MoS_2, and silicon into a heterostructure solar cell, one can take advantage of the strong light absorption of MoS_2, the ultrahigh charge carrier transport of graphene, and the stability of silicon-based photovoltaics. In this configuration, a Schottky junction forms between MoS_2 and n-type silicon, which enables efficient carrier separation, while graphene functions as an effective hole transport layer, facilitating carrier extraction. Recent studies have shown that optimizing the MoS_2 layer thickness can significantly modulate the Schottky barrier height, improve charge mobility, and enhance overall device performance (Singh, et al., 2017; Ma, et al., 2018; Borah, Tyagi and Kumar, 2020; Salih Omar, 2022).

It has been reported that the incorporation of graphene into MoS_2/n-Si solar cells significantly enhances external quantum efficiency (EQE) due to its exceptional optical transparency and conductivity. Despite the remarkable improvements in EQE, the overall power conversion efficiency (PCE) has been reduced. This reduction mainly comes from several factors, such as charge screening effects, where graphene's high

ARO-The Scientific Journal of Koya University
Vol. XIV, No.2 (2026), Article ID: ARO.12328. 7 pages
DOI: 10.14500/aro.12328
Received: 03 June 2025; Accepted: 29 July 2026
Regular research paper; Published: 19 September 2026
[†]Corresponding author's e-mail: omar.s.omar@uod.ac
Copyright © 2026 Omar S. Omar. This is an open access article distributed under the Creative Commons Attribution License (CC BY-NC-SA 4.0).

 http://dx.doi.org/10.14500/aro.12328

conductivity weakens the built-in electric field at the junction between the MoS_2 monolayer and n-silicon, subsequently hindering the efficiency of charge carrier separation and extraction. Moreover, interfacial trap states emerge at the heterojunction, creating additional recombination sites that further hinder performance (Wirth-Lima, Alves-Sousa and Bezerra-Fraga, 2019).

This study investigates these trade-offs by evaluating the impact of graphene incorporation on the performance of MoS_2/n-Si Schottky solar cells through detailed experimental analysis.

II. Materials and Methods

A. Growth of MoS_2 Monolayers

The MoS_2 monolayers were grown by low-pressure chemical vapor deposition using a single-zone (Elite Thermal Systems Ltd., UK) tube furnace equipped with Eurotherm 2416 PID and 2116 over-temperature controllers. The furnace has a maximum operating temperature of 1600°C with tunable ramping rates and heating zone of 45 cm. The inert gas flow was regulated by an MKS Type 1179A mass flow controller with a maximum flow rate of 1000 standard cubic centimeters per minute (SCCM). For the substrate, Silicon wafers with a thermally grown 300 nm SiO_2 layer on Si were purchased from MTI Corporation (1095 El Camino Real, Millbrae, CA 94030, USA). The wafers were cut into 1 × 2 cm^2 pieces using a diamond blade and cleaned with acetone before use to remove contaminants.

For the growth process, 300 mg of high-purity MoO_2 powder (99%, Sigma-Aldrich) was placed in a quartz boat and used as the molybdenum precursor. A cleaned SiO_2/Si substrate was positioned face-down above the MoO_2 container. The quartz boat containing the MoO_2 powder and substrate was loaded into the heating zone of the furnace. Another boat contained sulfur (10 mg, 99.98%, Sigma-Aldrich) placed at the inlet of tub s' furnace. Before the growth, the furnace was flushed with argon (1000 SCCM) to remove residual oxygen; then the furnace was ramped to the growth temperature of 800°C at a rate of 15°C/min under a continuous argon flow of 200 SCCM. The growth temperature was maintained at 800°C for 10–20 min, then naturally cooled down to room temperature.

B. MoS_2 Monolayers Characterization

The surface morphology of the as-grown MoS_2 monolayers was studied using a JEOL JSM-7800F Prime field emission scanning electron microscope (FESEM). The crystal morphology, surface coverage, and growth characteristics of the MoS_2 crystals grown on the SiO_2/Si substrates were investigated by FESEM analysis. The thickness of the MoS_2 monolayers was measured by NanoSurf Flex Axiom atomic force microscope (AFM). Photoluminescence (PL) measurements were performed on the MoS_2 monolayer film at room temperature under ambient conditions using a confocal Zeiss LSM 510 microscope with a 488 nm continuous-wave laser for excitation.

C. Transfer of Monolayer MOS_2 and Solar Cell Fabrication

The fabrication process of the Gr/MoS_2/n-Si solar cell is shown in Fig. 1. First, the native silicon oxide layer present on the surface of the n-type silicon wafer was removed by dipping it in a dilute hydrofluoric acid solution, then rinsing it in deionized water and drying it with nitrogen. This treatment exposed a clean silicon surface and minimized the interfacial oxide layer. The as grown Mos_2 monolayer film was transferred from the growth substrate onto the cleaned n-type Si using a poly (methyl methacrylate) (PMMA) assisted transfer technique. PMMA (950 K, Allresist GmbH, Germany) was spin-coated onto the MoS_2 surface to provide mechanical support during transfer. The underlying SiO_2 layer of the growth substrate was subsequently etched using Sodium hydroxide (NaOH) solution, releasing the PMMA/MoS_2 film. The detached PMMA/MoS_2 film was repeatedly rinsed in deionized water and pressed onto an n-type silicon wafer with <100> crystal orientation, resistivity of 1–5 Ω·cm, and thickness of 400 µm. After drying, the PMMA support layer was removed by dissolving it in ethanol, leaving the monolayer MoS_2 directly on the silicon surface.

Monolayer graphene provided by the State Key Laboratory of Silicon Materials, Zhejiang University, Hangzhou, China, was subsequently transferred onto the MoS_2/n-Si structure to form the graphene/MoS_2/n-Si heterojunction. Gold (Au) front electrodes were then deposited onto the graphene surface by thermal evaporation through a shadow mask. An indium–gallium (In–Ga) alloy was applied to the backside of the n-Si wafer to form an ohmic rear contact. The resulting

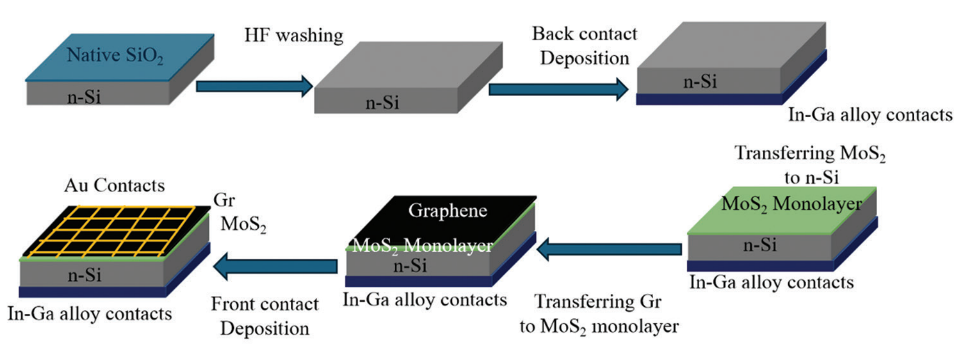

Fig. 1. Fabrication process of the Gr/MoS_2/n-Si solar cell.

device structure consisted of Au/Graphene/MoS_2/n-Si/In–Ga, completing the Gr/MoS_2/n-Si heterojunction solar cell.

D. Photovoltaic Characterization

The photovoltaic response of the fabricated Gr/MoS_2/n-Si heterojunction solar cells was measured under standard Air Mass 1.5 (AM 1.5) illumination. The illumination intensity was calibrated with a certified solar reference cell (PVM 937, PV Measurements Inc., USA).

Current–voltage (I–V) measurements were carried out using a solar-cell I–V data acquisition system (PV Measurements Inc., USA) in both dark and illuminated conditions. The measured current values were normalized to the active device area to obtain the respective current density-voltage (J-V) characteristics. The photovoltaic parameters, namely short-circuit current density (Jsc), open-circuit voltage (Voc), fill factor (FF), and PCE, were obtained from the J-V curves.

The EQE spectra were measured using a PVM QEXL solar-cell quantum-efficiency measurement system (PV Measurements Inc., USA), a fully integrated commercial platform for spectral response characterization, over the wavelength range of 300–1100 nm. The system employs a calibrated broadband light source and monochromator to generate wavelength-dependent illumination, while the resulting photocurrent is measured and compared with the incident photon flux to determine the EQE of the device. The EQE measurements were used to evaluate the wavelength-dependent photoresponse and carrier collection efficiency of the fabricated solar cells.

III. Results and Discussion

Our cardiovascular disease growth produced a large-scale, continuous monolayer of MoS_2, as shown in the low-resolution FESEM image Fig. 2. The left side (dark region) displays a continuous and uniform MoS_2 film with consistent contrast and morphology, while the right side (white regions) reveals the bare SiO_2/Si substrate sparsely decorated with isolated triangular MoS_2 crystals. The profound contrast difference between MoS_2 monolayers and the bare substrate

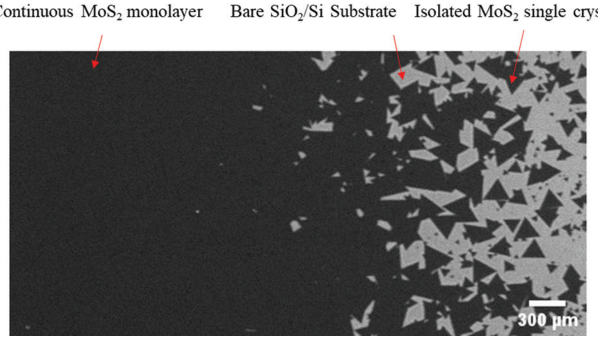

Fig. 2. Field emission scanning electron microscope micrograph showing a continuous monolayer of MoS_2 on the left side, right side displays the bare SiO_2/Si substrate, where isolated dark triangular domains of MoS_2 monolayers are spars.

comes from the variations in the secondary electron emission caused by the semiconducting and insulating characteristics of the monolayers and the substrate, respectively.

For Gr/MoS_2/n-Si heterojunction solar cell fabrication, the continuous film was selected, as the large, uniform, and continuous area is crucial for homogeneous contact interfaces, minimal recombination losses, and stable junction formation, which are critical for stable photovoltaic performance.

The monolayer thickness measurements were conducted by AFM. A small region of the film was gently scratched with a cotton swab to expose the underlying bare SiO_2/Si substrate, allowing direct step height analysis as shown in Fig. 3a, which clearly shows the boundary between the MoS_2 monolayer film and the bare substrate. The corresponding height profile in Fig. 3b, taken along the red line, reveals a step height of approximately 0.96 nm. This value lies within the reported thicknesses of monolayer MoS_2, which lie in the range of 0.8–1.0 nm (Li, et al., 2012).

PL measurements were carried out to explore the optical properties of the prepared MoS 2 monolayers. The monolayer PL spectrum in Fig. 4a was deconvoluted by Lorentzian peak fitting. Three peaks at 1.821 eV, 1.829 eV, and 1.972 eV correspond to the negatively charged A^- trion, neutral exciton A^0 and B exciton, respectively. The main A^- trion peak had a full width at half maximum (FWHM) of ~44 meV, and the main A^0 excitonic peak had an FWHM of ~47 meV, showing good optical quality of the synthesized monolayer. The simultaneous observation of well-resolved A^0 and $A^−$ emissions confirms that the MoS_2 film is a monolayer and indicates the presence of residual charge carriers in the material. Moreover, the relatively small linewidth of the A^0 exciton suggests a small inhomogeneous broadening and a moderate defect density.

The intensity ratio of the neutral exciton and the trion peak is a measure of the effect of charge doping. The emission of the lower-energy trion is a signature of the interaction between the excitons and free carriers. The observed positions of the peaks, their linewidth, and spectral features are in good agreement with the previously reported PL characteristics of MoS_2 monolayers (Mak, et al., 2010, 2013; Splendiani, et al., 2010).

PL mapping across the sample is shown in Fig. 4b. As can be seen, there is a spatially uniform PL emission intensity, suggesting excellent thickness uniformity and minimal strain or defect variation over the scanned area. These results are consistent with previous studies on monolayer MoS_2 films (Mak, et al., 2013).

The performance of graphene/MoS_2/n-Si heterostructure solar cells is mainly controlled by the optical absorption characteristics and carrier transfer and extraction efficiency of its components. MoS_2 monolayer has a direct band gap of 1.8 eV in the visible range, allowing for efficient electron-hole production (Salih Omar, 2022). Meanwhile, the electric field at the MoS_2/n-Si n-n-junction separates them. Electrons travel toward Si conduction band, and holes follow to the graphene layer, which acts as a transparent, high-mobility charge extraction layer (Ma and Shi, 2013; Ferrari, et al., 2015; Zhang, et al., 2020). The integration of

 http://dx.doi.org/10.14500/aro.12328

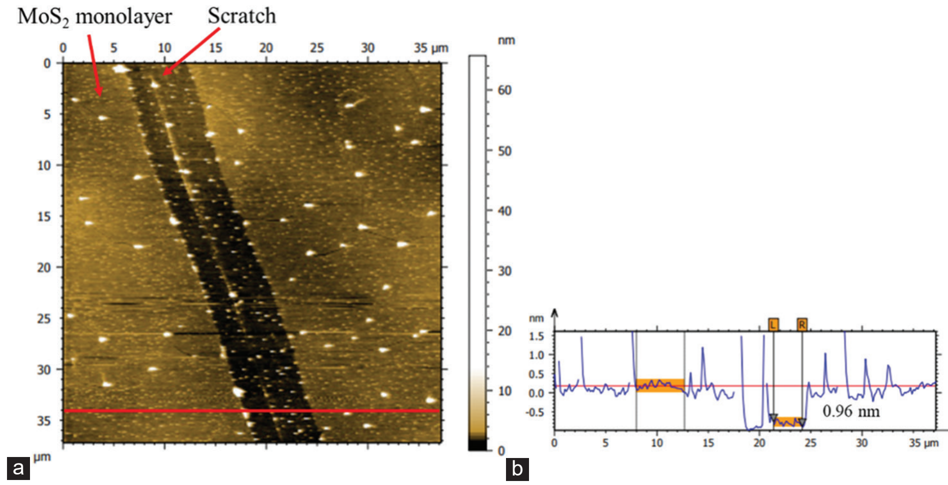

Fig. 3. (a) Atomic force microscope image of the MoS_2 monolayer film after mechanical scratching with a cotton swab to expose the underlying substrate. (b) The corresponding height profile was acquired along the red line across the scratched region.

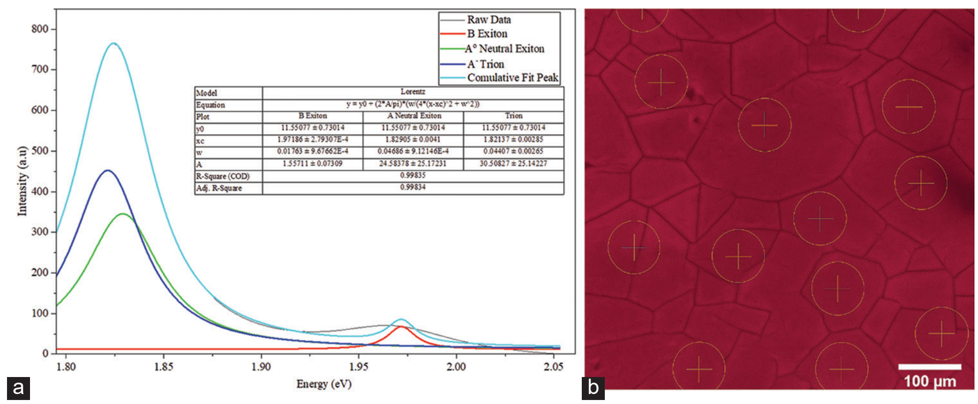

Fig. 4. (a): Room-temperature photoluminescence spectrum of the MoS_2 monolayer fitted with Lorentzian profiles. (b) PL intensity mapping over a selected area of the monolayer film.

graphene enhances photon absorption while at the same time changing the carrier transport characteristics. However, the exact impact of graphene addition on the carrier extraction is not fully clear without examining the J-V characteristics and EQE performance of the solar cell, which are discussed below.

Fig. 5 represents the J-V characteristics of the graphene/MoS_2/n-Si solar cell, which exhibits valuable insight into the charge transport behavior of the solar cell under study. In the dark, the J-V characteristics clearly exhibit a nearly constant current density of approximately -1.0×10^{-5} mA/cm^2 across both forward and reverse bias regions. The weak rectification behavior and high reverse current suggest poor Schottky barrier formation at the MoS_2-n-Si The weak rectification and the enhanced reverse current observed could be attributed to the modifications afforded by the graphene layer at the graphene/MoS_2 and MoS_2/n-Si interfaces. The residual contaminants, wrinkles, and interface defects during the graphene transfer process can create additional pathways for carrier transport, which results in increased leakage current. Moreover, charge transfer and Fermi-level pinning effects can change the interfacial energy-band alignment of graphene, resulting in a reduction of the effective Schottky barrier height. Although graphene can help carrier transport and improve carrier collection, these interfacial effects can simultaneously promote carrier recombination and non-radiative losses, thus deteriorating the diode characteristics of the junction (Rocha Robledo, et al., 2023).

This finding markedly differs from our previous observation on MoS_2/n-Si silicon solar cell, which clearly demonstrated strong rectification and diode-like behavior (Salih Omar, 2022).

Under illumination, the short-circuit current density (Jsc) increased to 19.95 mA cm^{-2} compared with 14.80 mA cm^{-2} for the previously reported monolayer-MoS^2/n-Si device (Salih Omar, 2022), indicating improved photocurrent generation and/or carrier collection. The open-circuit voltage (Voc) decreased from 0.314 to 0.199 V, while the FF decreased from 53.01% to 40.34%. These reductions, together with the weak rectification observed under dark conditions, indicate increased resistive, leakage, and recombination losses after graphene integration (Borah, Tyagi and Kumar, 2020; Rocha Robledo, et al., 2023; Fan, et al., 2024).

The EQE spectrum shown in Fig. 6 increases across the visible range, reaches a maximum of approximately 60% at 660 nm, remains broadly elevated to about 900 nm, and then

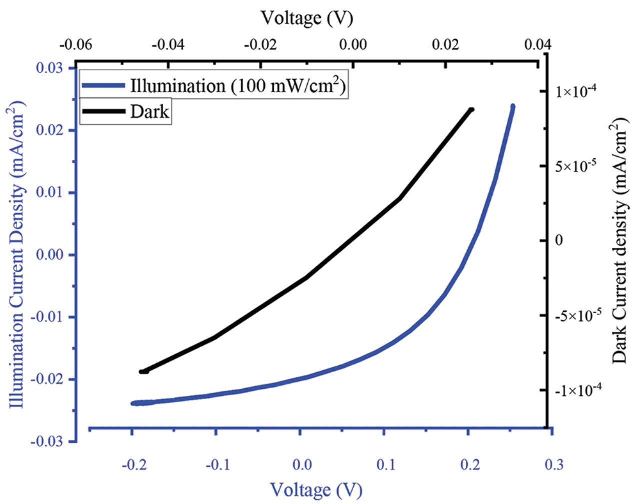

Fig. 5. J-V characteristics of Gr/MoS_2/n-Si Schottky solar cell under dark and illumination of 100 mW/cm[2].

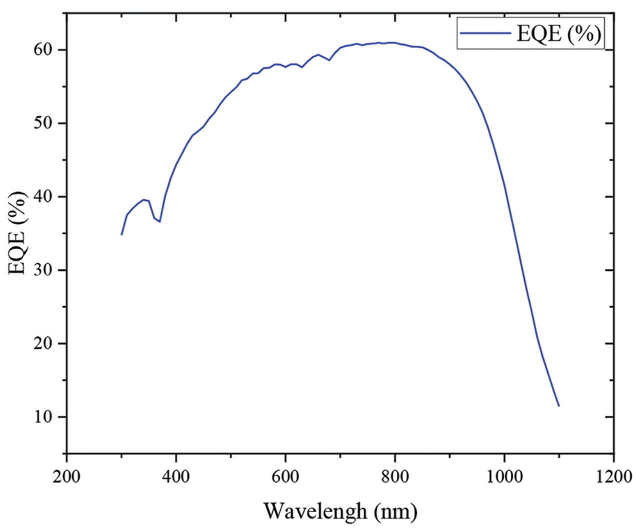

Fig. 6. External quantum efficiency spectra of Gr/MoS_2/n-Si Schottky solar cell.

declines at longer wavelengths. Compared with the maximum EQE of approximately 44% at 530 nm for the previously reported MoS_2/n-Si device (Salih Omar, 2022), the present graphene/MoS_2/n-Si structure exhibits an enhanced wavelength-dependent photocurrent response. This improvement may reflect the high optical transparency and carrier-transport properties of graphene; however, absorption and carrier-transfer processes were not measured independently, and their individual contributions cannot be conclusively separated (Bonaccorso, et al., 2015; Salih Omar, 2022).

While the EQE improved significantly, the overall conversion efficiency dropped from 2.46% to 1.60% (Salih Omar, 2022), indicating that carrier transport limitation outweighed the benefits of increased photon absorption. This mismatch implies that interfacial carrier recombination, current leakage pathways, and poor built-in electric potential adversely impact the carrier extraction efficiency in the solar cell (Song, et al., 2015).

Analyzing band alignment at the Gr/MoS_2/n-Si junction can give a better understanding of the charge transport, as illustrated by (Ma, et al., 2018). Prior to the graphene integration, the Schottky barrier height between MoS_2 monolayer-n-Si was relatively high (around 0.72 eV), causing effective carrier separation and negligible recombination losses. As MoS_2 has a higher conduction band minimum than the n-Si, it prevents photo-generated electrons from back-transferring to the silicon substrate. Simultaneously, its valence band maximum alignment facilitated effective hole transport.

Graphene addition lowered the Schottky barrier height to around ~0.65 eV, lowering injection resistance but at the same time promoting carrier recombination rates at the interface, causing a drop in the open-circuit voltage (from 0.34 to 0.199 V) and enhancing the leakage current. As graphene improved carrier transport properties, it also introduced band energetics modifications that contributed to non-radiative losses. Despite the EQE enhancement, the interfacial losses lowered the overall cell conversion efficiency (Ma, et al., 2018).

Another significant finding is the sharp decline in the shunt resistance after graphene insertion, from 6.96 kΩ for MoS_2/n-Si kΩ (Salih Omar, 2022) to 238 Ω for Gr/MoS_2/n-Si; such a reduction is another indicator of increased leakage current and high recombination rates. The smaller value of Shunt resistance suggests that while graphene improves photon absorption, it provides an additional carrier-loss pathway; this effect is exacerbated by weakened Schottky barrier control, which disrupts effective carrier separation and degrades device performance (Tsai, et al., 2014).

To place these results in the context of previously reported MoS_2/Si and graphene/MoS_2/Si photovoltaic devices, Table I compares the PCE, short-circuit current density (Jsc), open-circuit voltage (Voc), FF, and maximum EQE of the present device with closely related architectures.

The short-circuit current density of the present monolayer-graphene/monolayer-MoS_2/n-Si device is 19.95 mA cm^{-2}, which is higher than that of the previous graphene-free monolayer-MoS_2/n-Si device (14.80 mA cm^{-2}) and the single-layer-graphene/~17 nm MoS_2/n-Si device reported by (Tsuboi, et al., 2015) (13.10 mA cm^{-2}), as shown in Table I. However, the present device exhibits a much lower open-circuit voltage and FF compared to those reference devices. Therefore, the enhancement of photocurrent response does not result in an increase in PCE.

Tsuboi et al. (2015) show that the number of graphene layers and the MoS_2 interlayer thickness strongly affect the performance. The efficiency increased from 1.35% to 8.02% by increasing the graphene layer number from one to three at a MoS_2 thickness of ~17 nm, and further to 11.1% by reducing the MoS2 thickness to ~9 nm. The optimized device achieved Jsc = 33.4 mA cm^{-2}, Voc = 0.56 V, and FF = 60%. These results suggest that the reduced efficiency of the present device cannot be simply attributed to the use of graphene, but the quality of the interfaces and the optimization of the graphene and MoS 2 layers are crucial (Tsuboi, et al., 2015).

Ma et al. also reported similar thickness dependence. The MoS_2 interlayer is controlled to be ~4 nm (six-layer), and the

http://dx.doi.org/10.14500/aro.12328

TABLE I
COMPARISON OF THE PHOTOVOLTAIC PERFORMANCE OF THE PRESENT GRAPHENE/MoS_2/N-SI SOLAR CELL WITH PREVIOUSLY REPORTED GRAPHENE/MoS_2/SI AND RELATED MoS_2/SI DEVICES

Device architecture	Important design details	PCE (%)	Jsc (mA cm^{-2})	Voc (V)	FF (%)	Maximum EQE	References
Monolayer MoS_2/n-Si	CVD-grown MoS_2 monolayer transferred onto n-Si	2.46	14.80	0.314	53.01	44% at 530 nm	(Salih Omar, 2022)
Monolayer graphene/monolayer MoS_2/n-Si	Sequential PMMA-assisted transfer; no intentional graphene doping	1.60	19.95	0.199	40.34	60% at 660 nm	This work
Single-layer graphene/~17 nm MoS_2/n-Si	CVD-grown multilayer MoS_2 transferred by thermal-release tape	1.35	13.10	0.410	25.0	NR	(Tsuboi, et al., 2015)
Trilayer graphene/~17 nm MoS_2/n-Si	Same MoS_2 thickness; graphene layer number increased to three	8.02	28.2	0.540	53.0	NR	(Tsuboi, et al., 2015)
Trilayer graphene/~9 nm MoS_2/n-Si	Optimized thinner MoS_2 interlayer	11.10	33.4	0.560	60.0	NR	(Tsuboi, et al., 2015)
Graphene/~4 nm (6L) MoS_2/n-Si	Layer-controlled MoS_2; no TiO_2 antireflection coating	13.10	32.8	0.590	68.0	NR	(Ma, et al., 2018)
Graphene/~4 nm (6L) MoS_2/ n-Si+TiO_2	Same optimized device with a TiO_2 antireflection coating	15.80	36.8	0.590	73.0	NR	(Ma, et al., 2018)
Monolayer MoS_2/p-Si	Large-area CVD MoS_2 monolayer forming a type-II heterojunction	5.23	22.36	0.410	57.26	NR	(Tsai, et al., 2014)
Bulk-like MoS_2/p-Si	~40 nm sputtered MoS_2 film; measured at 15 mW cm^{-2} illumination	1.30	3.20	0.140	42.4	NR	(Hao, et al., 2015)

NR: Not reported as a numerical maximum in the cited source. PCE: Power conversion efficiency, CVD: Cardiovascular disease

efficiency of the graphene/MoS 2/n-Si device is 13.1% before optical treatment. The application of a TiO_2 antireflection coating on the Ag/SiN_x/Si solar cell increased the Jsc from 32.8 to 36.8 $mAcm^{-2}$ and FF from 68% to 73% resulting in a final efficiency of 15.8% with Voc remaining at 0.59 V. Thus, the maximum literature value in Table I is the result of a cumulative effect of MoS_2 thickness optimizations, better interfacial carrier selectivity, and antireflection management, not just the graphene/MoS2/Si architecture (Ma, et al., 2018).

Related MoS_2/Si devices also highlight the junction quality and measurement conditions. Tsai et al. reported the fabrication of a type-II heterojunction based on monolayer-MoS_2/p-Si with an efficiency of 5.23% with Jsc = 22.36 mA cm^{-2}, Voc = 0.41 V, and FF = 57.26% (Tsai, et al., 2014). For comparison, the bulk-like sputtered MoS_2/p-Si junction by Hao et al. achieved 1.3% efficiency under much lower illumination intensity of 15 mW cm^{-2}. The latter result is not intended for direct comparison to one-sun AM 1.5G measurements, but to illustrate the influence of device structure, film thickness, interface formation, and test conditions on the reported photovoltaic metrics (Hao, et al., 2015).

The low Voc of 0.199 V, FF of 40.34%, weak dark rectification, and low shunt resistance for the present device suggest that the benefit of the increased photocurrent is offset by leakage and interfacial recombination. Transfer residues, wrinkles, partial surface reoxidation, and imperfect contact formation may be contributing factors. However, the graphene work function, interface-state density, and Schottky barrier height were not directly measured, so these mechanisms should be presented as plausible interpretations and not confirmed causes.

IV. CONCLUSION

The Gr/MoS_2/n-Si device exhibited a maximum EQE of 60% at approximately 660 nm and a broad spectral response from about 660 to 900 nm, indicating enhanced wavelength-dependent photocurrent generation compared with the graphene-free MoS_2/n-Si reference. Nevertheless, the PCE decreased from 2.46% to 1.60%, Voc decreased to 0.199 V, and the shunt resistance declined to 238 Ω. These results show that interfacial recombination and leakage losses outweighed the benefit of the improved photocurrent response. Future work should focus on cleaner transfer, interface passivation, controlled graphene work-function modification, and optimization of the graphene and MoS_2 layer thicknesses to improve Voc, FF, and overall efficiency.

V. ACKNOWLEDGMENT

The author would like to acknowledge Dr. Kun Huang from Zhejiang University and Prof. Dr. Jun Yuan from the University of York for scientific discussions and experimental support related to this work.

The Kurdistan Regional Government's Human Capacity Development Program provided funding for this research.

REFERENCES

Amani, M., Lien, D.H., Kiriya, D., Xiao, J., Azcatl, A., Noh, J., Madhvapathy, S.R., Addou, R., Santosh, K.C., Dubey, M., Cho, K., Wallace, R.M., Lee, S.C., He, J.H., Ager, J.W.3rd., Zhang, X., Yablonovitch, E., and Javey, A., 2015. Near-unity photoluminescence quantum yield in MoS_2. *Science*, 350(6264), pp.1065-1068.

Bonaccorso, F., Colombo, L., Yu, G., Stoller, M., Tozzini, V., Ferrari, A.C., Ruoff, R.S., and Pellegrini, V., 2015. 2D materials. Graphene, related two-dimensional crystals, and hybrid systems for energy conversion and storage. *Science,* 347(6217), p.1246501.

Borah, C.K., Tyagi, P.K., and Kumar, S., 2020. The prospective application of a graphene/MoS_2 heterostructure in Si-HIT solar cells for higher efficiency. *Nanoscale Advances*, 2(8), pp.3231-3243.

Du, X., Skachko, I., Barker, A., and Andrei, E.Y., 2008. Approaching ballistic transport in suspended grapheme. *Nature Nanotechnology*, 3(8), pp.491-495.

Fan, K., Zhou, S., Xie, L., Jia, S., Zhao, L., Liu, X., Liang, K., Jiang, L., and Kong, B., 2024. Interfacial assembly of 2D graphene-derived ion channels for water-based green energy conversion. *Advanced Materials*, 36(9), p.e2307849.

Ferrari, A.C., Bonaccorso, F., Fal'ko, V., Novoselov, K.S., Roche, S., Bøggild, P., Borini, S., Koppens, F.H., Palermo, V., Pugno, N., Garrido, J.A., Sordan, R., Bianco, A.,… & Kinaret J., 2015. Science and technology roadmap for graphene, related two-dimensional crystals, and hybrid systems. *Nanoscale*, 7(11), pp.4598-4810.

Hao, L., Liu, Y., Gao, W., Han, Z., Xue, Q., Zeng, H., Wu, Z., Zhu, J., and Zhang, W., 2015. Electrical and photovoltaic characteristics of MoS2/Si *p-n* junctions. *Journal of Applied Physics*, 117(11), p.114502.

Li, H., Zhang, Q., Ray Yap, C.C., Tay, B.K., Edwin, T.H.T., Olivier, A., and Baillargeat, D., 2012. From bulk to monolayer MoS_2: Evolution of Raman scattering. *Advanced Functional Materials*, 22(7), pp.1385-1390.

Ma, J., Bai, H., Zhao, W., Yuan, Y., and Zhang, K., 2018. High efficiency graphene/MoS_2/Si Schottky barrier solar cells using layer-controlled MoS 2 films. *Solar Energy*, 160, pp.76-84.

Ma, X.Y., and Shi, M.Y., 2013. Study of the electrical contact properties of monolayer MoS_2/Si heterojunction. *Advanced Materials Research*, 660, pp.57-60.

Mak, K.F., He, K., Lee, C., Lee, G.H., Hone, J., Heinz, T.F., and Shan, J., 2013. Tightly bound trions in monolayer MoS_2. *Nature Materials*, 12(3), pp. 207-211.

Mak, K.F., Lee, C., Hone, J., Shan, J., and Heinz, T.F., 2010. Atomically thin MoS_2: A new direct-gap semiconductor. *Physical Review Letters*, 105(13), p.136805.

Novoselov, K.S., Fal'ko, V.I., Colombo, L., Gellert, P.R., Schwab, M.G., and Kim, K., 2012. A roadmap for graphene. *Nature*, 490(7419), pp.192-200.

Rao, R., Islam, A.E., Singh, S., Berry, R., Kawakami, R.K., Maruyama, B., and Katoch, J., 2019. Spectroscopic evaluation of charge-transfer doping and strain in graphene/MoS_2 heterostructures. *Physical Review. B*, 99(19), p.195401.

Rocha Robledo, A.K., Flores Salazar, M., Muñiz Martínez, B.A., Torres-Rosales, Á.A., Lara-Alfaro, H.F., Del Pozo-Zamudio, O., Cerda-Méndez, E.A., Jiménez-Sandoval, S., and De Luna Bugallo, A., 2023. Interlayer charge transfer in supported and suspended MoS2/Graphene/MoS_2 vertical heterostructures. *PLoS One*, 18(7), p.e0283834.

Salih Omar, O., 2022 Monolayer MoS2/n-Si heterostructure Schottky solar cell. *Journal of Renewable Materials*, 10(7), pp.1979-1988.

Singh, E., Kim, K.S., Yeom, G.Y., and Nalwa, H.S., 2017. Atomically thin-layered molybdenum disulfide (MoS_2) for bulk-heterojunction solar cells. *ACS Applied Materials and Interfaces*, 9(4), pp.3223-3245.

Song, Y., Li, X., Mackin, C., Zhang, X., Fang, W., Palacios, T., Zhu, H., and Kong, J., 2015. Role of interfacial oxide in high-efficiency graphene-silicon Schottky barrier solar cells. *Nano Letters*, 15(3), pp.2104-2110.

Splendiani, A., Sun, L., Zhang, Y., Li, T., Kim, J., Chim, C.Y., Galli, G., and Wang F., 2010. Emerging photoluminescence in monolayer MoS_2. *Nano Letters*, 10(4), pp.1271-1275.

Tao, H., Fan, Q., Ma, T., Liu, S., Gysling, H., Texter, J., Guo, F., and Sun, Z., 2020. Two-dimensional materials for energy conversion and storage. *Progress in Materials Science*, 111(100637), p.100637.

Tsai, M.L., Su, S.H., Chang, J.K., Tsai, D.S., Chen, C.H., Wu, C.I., Li, L.J., Chen, L.J., and He, J.H., 2014 Monolayer MoS2 heterojunction solar cells. *ACS Nano*, 8(8), pp.8317-8322.

Tsuboi, Y., Wang, F., Kozawa, D., Funahashi, K., Mouri, S., Miyauchi, Y., Takenobu, T., and Matsuda, K., 2015. Enhanced photovoltaic performances of graphene/Si solar cells by insertion of a MoS_2 thin film. *Nanoscale*, 7(34), pp.14476-14482.

Wirth-Lima, A.J., Alves-Sousa, P.P., and Bezerra-Fraga, W., 2019. Graphene/silicon and 2D-MoS_2/silicon solar cells: A review. *Applied Physics. A,* 125(4), p.241.

Zhang, Y., Su, P., Liu, L., Qiu, P., Su, L., Fu, G., and Yu, W., 2020. The effect of MoS_2 modulated doping with molybdenum-oxide on the photovoltaic performance for MoS_2/n-Si heterojunction solar cells. *Solar Energy*, 208, pp.1048-1057.